OXYGEN ISOTOPES IN FINE-GRAINED SPINEL-PYROXENE AND MELILITE-RICH CAIs IN THE ALHA 77307 CO3.0 CARBONACEOUS CHONDRITE. B. Jacobsen[1], J. M. Han[2], J. E. Matzel[1], A. J. Brearley[2], and I. D. Hutcheon[1], [1]Lawrence Livermore National Laboratory, 7000 East Ave, Livermore, CA 94550, USA (jacobsen5@llnl.gov), [2]Department of Earth and Planetary Sciences, MSC03-2040, University of New Mexico, Albuquerque, NM 87131, USA. (e-mail: jmhan@unm.edu).

Introduction: The origin and evolution of oxygen isotope in the early solar system provide important constraints on the physical and chemical processes that occurred during the lifetime of the proto-planetary disk. The general model for explaining the observed O-isotope variations assumes that the O-isotope compositions of both gas and early-forming solids were initially ^{16}O-rich ($\Delta^{17}O \leq -25‰$), similar to the recently reported value for the Sun ($\Delta^{17}O = -28‰$) [1], and evolved with time as a result of CO self-shielding and/or dust-gas fractionation [2−5].

Recent high spatial resolution O-isotope measurements of the Wark-Lovering (WL) rim and margin of an Allende CAI showed large variations in $\Delta^{17}O$ of ~25‰, suggesting mixing between an ^{16}O-rich solar environment and an ^{16}O-poor reservoir and exposure of CAIs to distinct nebular O-isotope reservoirs by transfer among different environments within the proto-planetary disk [6]. However, interpretation of O-isotopes in Allende CAIs, in particular, is complicated due to the extensive history of thermal metamorphism and alteration on the Allende parent body. The effects of parent body alteration on O-isotope variations are difficult to constrain.

Petrologic studies of CAIs and AOAs within ALHA 77307, a pristine CO3 chondrite, suggest transport of early-condensed solids into hotter region of the nebula that had undergone only partial condensation, followed by back-reaction of solids with the nebular gas [7]. The microstructures of these inclusions, as well as the pristine nature of the chondrite, in general, indicate that the inclusions have not undergone any post-accretion alteration. Although the refractory inclusions show evidence of disequilibrium reactions, each inclusion appears to have experienced a unique formation and thermal history. Thus, variations in O-isotopes can be directly linked to an evolving gas composition.

To investigate the suggestion that the complex thermal history observed in CAIs and AOAs in ALHA 77307 reflects transport of these objects through ^{16}O-rich and ^{16}O-poor nebular regions, we analyzed the oxygen isotope compositions in two fine grained CAIs in the ALHA 77307 CO3.0 carbonaceous chondrite.

CAI Petrography: CAIs from a thin section of the ALHA 77307 CO3.0 chondrite were initially investigated in detail by elemental X-ray mapping and BSE imaging using a FEI Quanta 3D FEG-SEM/FIB operating at 30 kV at UNM. The two main types of CAIs are: (1) spinel-pyroxene inclusions and (2) melilite-rich inclusions [7, 8].

Spinel-pyroxene CAI (RI 065) is a mineralogically-zoned object (190 μm × 230 μm in size) that has sub-rounded to elongated spinel cores rimmed by a ~5-20 μm-thick layer of diopside, sometimes followed by a partial layer of fosterite olivine. A complex layer of intergrown spinel and diopside occurs between the spinel cores and diopside rims. Minor melilite ~50 μm across is present in a region between the different spinel cores. Pores usually occur around and within the spinel cores.

Melilite-rich CAI (RI 054) is a rounded object, ~110 μm in diameter. This inclusion consists of a compact melilite-rich core (~70 μm in diameter) with minor perovskite and spinel, enclosed by ~25 μm-wide porous zone which consists of a complex intergrowth of fine-grained melilite, spinel, and perovskite. The outer rim of the inclusion consists of a discontinuous layer of diopside up to ~2.5 μm thick [7, 8].

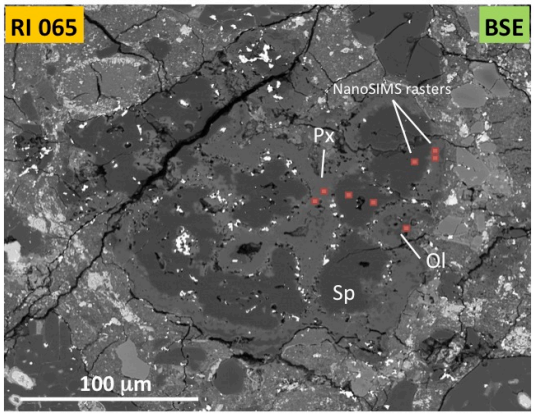

Figure 1. Backscattered electron image of RI 065. Px = pyroxene; Sp = spinel, Ol = olivine. Red squares denote areas analyzed by the NanoSIMS.

Based on the microstructural characteristics of RC 054, Han and Brearley [8] suggested that this inclusion had undergone back-reaction with a nebular gas under disequilibrium conditions, resulting in the complex porous intergrowth of melilite, spinel and perovskite. Such disequilibrium reactions could be the result of transport of the inclusion into regions of the nebular disk that was at higher temperatures and may have had

a distinct oxygen isotopic composition from the primary equilibrium condensate phases.

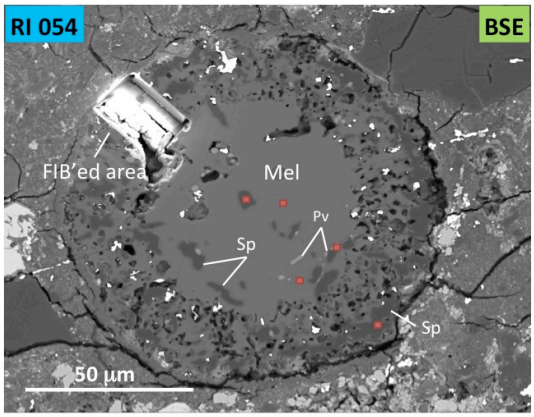

Figure 2. Backscattered electron image of RI 065. Mel = melilite; Sp = spinel, Pv = perovskite. Red squares denote areas analyzed by the NanoSIMS.

Methods: The oxygen isotopic composition of the CAIs was measured at the Lawrence Livermore National Laboratory using a *Cameca* NanoSIMS 50. The protocol for measuring oxygen isotopes follows [6, 9]. A ~10 pA Cs+ primary beam with a diameter of ~200 nm was rastered over 2×2 μm^2 areas Negative secondary ions were acquired by simultaneously measuring $^{16}O^-$ on a Faraday cup and $^{17}O^-$, $^{18}O^-$, and $^{28}Si^-$ on electron multipliers. A mass resolving power of ~7000 was used to minimize the contribution from $^{16}OH^-$ to $^{17}O^-$. Instrumental mass fractionation was determined by measuring matrix matched terrestrial standards. The external reproducibility of our standards on $\Delta^{17}O$ was <6‰ (2σ).

Results: Oxygen isotope data were collected for different mineral phases across CAIs RI 065 and RI 054. The two CAIs are uniformly ^{16}O-rich ($\Delta^{17}O \approx -22$‰); no systematic discernable differences in oxygen isotope abundances, outside the analytical uncertainty, between the distinctive mineral phases are observed (Fig. 3). The total range in $\Delta^{17}O$ is within the analytical uncertainty: between −23.1‰ and −21.1‰ for RI 065 and RI 054 −23.4‰ and −20.5‰,. The average $\Delta^{17}O$ for RI 065 and RI 054 is −22.4 ± 1.7‰ and −21.6 ± 2.8‰, respectively. In contrast, data for a chrondrule located in the same thin section as the CAIs show a distinctly ^{16}O-poor composition with $\Delta^{17}O \sim -5$‰.

Conclusions: Unlike data from the rims of igneous CAIs in CV chondrite, our data suggest that despite convincing petrographic evidence for complex formation and thermal history, the CAIs in ALHA 77307 did not react and/or re-equilibrate with an ^{16}O-poor nebular gas subsequent to their formation. Any interaction with the nebular gas that resulted in the formation of the distinct reaction textures in these inclusions must have occurred in a reservoir with the same oxygen isotopic composition as the primary condensate phases. The inclusions do not, therefore, record direct isotopic evidence of transport within the protoplanetary disk. Our data are consistent with previous data for unmelted fine-grained CAIs in the CO3.0 carbonaceous chondrite Yamato-81020 that have uniform $\Delta^{17}O \approx -22$ ‰ [10] and support a scenario in which mineralogical and, to some extent, chemical, alteration of CAIs in the least metamorphosed CO chondrites is decoupled from O-isotope exchange. In this regard, the record of CAIs in CO3 chondrites is similar to that of CAIs in CM chondrites [9]. The distinct $\Delta^{17}O$ value for the ALHA 77307 chondrule suggests chondrules in the CO chondrites formed in a region of the nebula similar to chondrules from CV chondrites and that mixing of ^{16}O-rich and ^{16}O poor components occurred at low temperatures after the end of metamorphic processing.

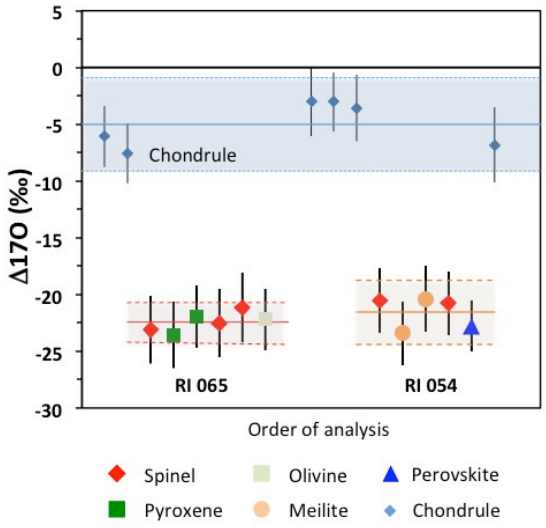

Figure 2. Showing D17O for distinct mineral phases in RI 065 and RI 054 from ALHA77307. Also shown are data from a chondrule close to the CAIs.

References: [1] McKeegan, K. D. et al., (2011) *Science,* 332, p. 1528–1532. [2] Aléon, J. et al. (2007) *EPSL,* 263, 114–127. [3] Clayton, R. N. (2002) *Nature*, 415, 860–861. [4] Krot, A. N. et al (2005) *ApJ*, 622, 1333–1342. [5] Lyons, J. R. and Young, E. D. (2005) *Nature*, 435, 317–320. [6] Simon, J. I. et al. (2011) *Science,* 331, 1175–1178. [7] Han, J. M. and Brearley, A. J. (2012) *LPSC XXXXIII*, Abstract #1324. [8] Han, J. M. and Brearley, A. J. (2013) *LPSC XXXXIV*, Abstract #2682. [9] Matzel, J. E. P. et al. (2013) *LPSC XXXXIV*, Abstract #2632. [10] Itoh, S. et al. (2004) *GCA,* 68, 183–194.